Astron. Astrophys. 273, 533–545 (1993)

ASTRONOMY AND ASTROPHYSICS

Unified NLTE model atmospheres including spherical extension and stellar winds

IV. Improved line transfer and wind contamination of H, He profiles

F. Sellmaier[1], J. Puls[1], R.P. Kudritzki[1,2], A. Gabler[1], R. Gabler[1], and S.A. Voels[1]

[1] Institut für Astronomie und Astrophysik, Scheinerstr. 1, W-8000 München 80, Germany
[2] Max-Planck-Institut für Astrophysik, Karl-Schwarzschild-Str. 1, W-8046 Garching, Germany

Received November 13, 1992; accepted March 8, 1993

Abstract. The treatment of NLTE multilevel radiative transfer in the presence of sub- and supersonic velocity fields of unified model atmospheres is discussed. The solution of the line transfer in the comoving frame is obtained via Accelerated Λ-Iteration where we apply the new Approximate Λ-Operator developed by Puls (1991). This method yields excellent convergence also in cases of very complex model atoms, where many strong, intermediate and weak lines have to be treated simultaneously and where other operators failed to achieve convergence.

This algorithm is used to investigate the contamination of photospheric hydrogen and helium absorption lines by emission of the stellar wind. It is found that in the case of early O-supergiants close to the Eddington-limit wind contamination is significant and leads to systematic errors in the determination of stellar parameters, if purely hydrostatic, plane parallel NLTE models are used for the spectral analysis.

Additionally, a specific behavior of the mean line intensity, namely a local minimum around the sonic point, is discussed by means of a second order Sobolev Approximation accounting for curvature terms in the velocity field.

Key words: stars: atmospheres – line formation – stars: early type – stars: emission lines – stars: mass loss

1. Introduction

The most luminous stars in galaxies are very massive supergiants of spectral type O, B, A. With the forthcoming new generation of very large ground-based telescopes and the corrected Hubble Space Telescope it will be possible to study the spectra of such objects quantitatively in galaxies far beyond the Local Group. In this way, chemical abundances and, even more important, distances of galaxies can be determined by new independent methods (Kudritzki et al. 1992).

Unfortunately, the task of quantitative spectroscopy of very massive, hot supergiants is not an easy one. Severe departures from LTE and hydrodynamic effects inferred by the radiation driven winds of these objects affect the determination of stellar parameters and abundances. Consequently, a considerable effort is needed to model the atmospheres of such stars (for a recent review, see Kudritzki & Hummer 1990).

One possible way for the quantitative spectroscopy of blue, luminous supergiants is the concept of "Unified model atmospheres" introduced by Gabler et al. (1989, Paper I). This new type of NLTE model atmospheres includes the spherical extension of supergiant atmospheres and their stellar winds in combination with a smooth transition into the subsonic photospheres. In two recent papers (Gabler et al. 1991 (Paper II), Gabler et al. 1992 (Paper III)) it was demonstrated that unified models provide a much better description of the EUV radiation field of hot stars than the classical plane parallel, hydrostatic NLTE models. In this paper we deal with the line transfer for the calculation of synthetic spectra.

The concept of unified model atmospheres, as introduced in Paper I, combines three subsequent steps. First, density structure and velocity field are calculated from the hydrodynamic equations of radiation driven winds in the entire sub- and supersonic atmosphere. Second, NLTE opacities and emissivities of hydrogen and helium are used in the energy equation of radiative equilibrium to calculate the temperature stratification in the entire atmosphere. In this step, only the most important bound-free and free-free transitions are included and the line transfer is treated in the Sobolev approximation. Therefore, a third step is needed for the calculation of synthetic spectra, in which very detailed and complex model atoms are taken into account and an accurate solution of the multiline NLTE radiative transfer problem is required.

This paper concentrates on the third step and investigates several different methods for the calculation of synthetic line

Send offprint requests to: F. Sellmaier

spectra emitted by the sub- and supersonic regions of unified model atmospheres. In Sect. 2 we describe the general requirements for the line transfer in unified models and the numerical difficulties that have been encountered in the past. We analyze these difficulties and discuss several numerical methods to achieve convergence for the iterative line transfer problem. The best algorithm is selected to converge exact solutions of the radiation field in the entire sub- and supersonic atmosphere. In Sect. 3 we use this exact solution to describe the properties of the mean line intensity around the sonic point – the most critical region for line radiation transfer – and compare it with commonly used approximative methods. In Sect. 4 we apply our exact method to investigate the problem of the contamination of photospheric absorption line profiles by emission of the surrounding stellar wind and discuss the consequence of this effect for the determination of stellar parameters.

2. Improving the convergence of line formation

As described in Paper I, spectral lines of mass losing luminous stars are formed in both atmospheric regions, the subsonic photosphere and the supersonic stellar wind. Therefore, a formalism is needed that describes the line radiation transfer in both regions with the same accuracy. After the paper by Mihalas et al. (1975) it has become clear that the best treatment (in case of a monotonic velocity field) is to transform the problem into the comoving frame (CMF) of the wind, to solve the complete rate and transfer equations in this frame and then to transform back into the observer's frame. An alternative, very common method to solve the line transfer in expanding atmospheres is the so called Sobolev Approximation (Sobolev 1957). This approach saves an enormous amount of computer time, but, as we will show in Sect. 3, it is not sufficient for most of our problems.

In our approach, the multi line NLTE problem is treated iteratively by applying the method of the Accelerated Lambda Iteration (ALI) by Werner & Husfeld (1985) which uses a perturbation approach (Cannon 1973) to avoid the extremly slow convergence of the Lambda Iteration. In the ordinary Lambda Iteration the mean line intensity is the quantity which couples line transfer and rate equations and is defined as an integral over frequency ν

$$\overline{J} = \int \varphi_\nu \, J_\nu \, d\nu = \Lambda[S_L] \tag{1}$$

with J_ν the mean intensity and φ_ν the normalized profile function[1]. Note that we define Λ to operate on the line source function only and include the continuum source function in an (approximately) constant offset (cf. Eq. (5). The ALI method replaces $\overline{J}$ in the n-th iteration by

$$\overline{J}^n := \Lambda^* \cdot S_L^n + (\Lambda[S_L^{n-1}] - \Lambda^* \cdot S_L^{n-1}). \tag{2}$$

The upper indices denote the iteration cycle and Λ^* is the so called *Approximate Lambda Operator* (ALO) which has to be local in this formulation. Hence, the approximate solution for $\overline{J}^n$ and S_L^n can be found directly and just the "perturbation" term $(\Lambda[S_L^{n-1}] - \Lambda^* \cdot S_L^{n-1})$ has to be iterated.

For this purpose Eq. (2) is inserted into the radiative rates, which are redefined subsequently[2]. Together with the definition of a local ALO Λ^* the usual form to redefine the rates are *effective radiative rates* which remove the contribution of the local radiation field at optically thick frequencies from the rate equations. The effective rates in the n-th iteration are then given by

$$\begin{aligned} R_{ij}^{\text{eff}} &:= B_{ij}\overline{J}^{\text{eff}} := B_{ij}(\Lambda - \Lambda^*)[S_L^{n-1}] \\ R_{ji}^{\text{eff}} &:= A_{ji}(1 - \Lambda^*) + B_{ji}\overline{J}^{\text{eff}} \\ &:= A_{ji}(1 - \Lambda^*) + B_{ji}(\Lambda - \Lambda^*)[S_L^{n-1}] \end{aligned} \tag{3}$$

where the local contribution of the line source function, i.e. $\Lambda^* S_L$, has been eliminated by inserting $S_L = n_j A_{ji}/(n_i B_{ij} - n_j B_{ji})$ into the original rates.

With view on Eq. (2) one sees immediately that the solution $\overline{J} = \Lambda[S_L]$ is found once the iteration has achieved convergence, i.e. $S_L^n - S_L^{n-1} \to 0$. The solution is independent from the value of Λ^*. However, the critical point of the ALI is to achieve convergence at all, i.e. to find the appropriate ALO Λ^*. In paper I, the "core fraction operator" introduced by Hamann (1985) was used as ALO for the CMF transfer with satisfactory numerical success. But as the complexity of the model atoms was increased (in particular, by introducing a detailed He I model atom) so that very strong, intermediate and a large number of weak lines had to be treated simultaneously, severe convergence problems were encountered in the region around the sonic point. We were therefore forced to investigate this problem and to provide a new solution. This procedure is described in the following subsections.

The examples given in this and the following section are calculated for a unified model with the parameters T_{eff}= 42 000 K, log g= 3.5, $R_\star/R_\odot$ = 18, N_{He}/N_H = 0.1 and $\dot{M}$= 9.9 $\cdot 10^{-6} M_\odot$/yr. However, the statements given in this section are tested for mass-loss rates from 1 to 30 $\cdot 10^{-6} M_\odot$/yr.

2.1. A criterion for convergence

The reason for success and failure of an ALO was examined by Puls & Herrero (1988). They proved the suggestion by Olson et al. (1986), that the best choice for a *local* ALO Λ^* is the diagonal of the Λ-matrix,

$$\underline{\underline{\Lambda}}^* := diag(\underline{\underline{\Lambda}}'), \tag{4}$$

where $\underline{\underline{\Lambda}}'$ represents the linear part of the complete Λ operator, i.e. the part which acts on the line source function only. The

[1] Here and in following we assume complete redistribution

[2] In principle, we may define any new radiative rates R'_{ij} and R'_{ji} (used alternatively to the common quantities R_{ij}, R_{ji}), as long as the corresponding net rates are identical, i.e. $n_i R'_{ij} - n_j R'_{ji} = n_i R_{ij} - n_j R_{ji}$.

discretized form of the complete line transfer equation is an affine $ND \times ND$ matrix equation (ND: number of depth points),

$$\underline{\overline{J}} = \underline{\Phi} + \underline{\underline{\Lambda}}' \cdot \underline{S}_L \tag{5}$$

where the offset $\underline{\Phi}$ is due to the inner boundary condition and the opacity and emissivity of overlapping continua and $\underline{\underline{\Lambda}}'$ represents the actual transfer of the line source function. The vectors $\underline{\overline{J}}$ and $\underline{S}_L$ contain the mean line intensity and the line source function, respectively, at each depth point.

Puls & Herrero showed that the use of the ALO $\underline{\underline{\Lambda}}^* = diag(\underline{\underline{\Lambda}}')$ will always lead to convergence of the line transfer problem. However, in case of the CMF line transfer the determination of the exact diagonal requires the solution of the transport equations to be peformed ND times which is much too time-consuming and thus an approximation is necessary. For similar reasons, Puls & Herrero estimated the limits in which the exact diagonal can be *approximated* without producing divergence. They considered the pure line transfer (fixed continuum opacities) and approximated the rate equations, $S_L = F[\overline{J}]$, by

$$S_{L\,i} \approx \Psi_i + \xi_i \cdot \overline{J}_i \qquad (i = 1..ND). \tag{6}$$

Then the limits in which a local ALO $\underline{\underline{\Lambda}}^*$ yields convergence are

$$0 < \Lambda^*_{ii} < \Lambda'_{ii} + \frac{1-\xi_i}{2\xi_i} \qquad (i = 1..ND). \tag{7}$$

In the case that radiative rates dominate, ξ_i is close to unity so that the range where Λ'_{ii} can be overestimated is very small. If Λ'_{ii} is underestimated, convergence is guaranteed, but the smaller the Λ^*_{ii}, the slower the rate of convergence, ending up in ordinary Λ-iteration for $\Lambda^*_{ii} = 0$.

It should be mentioned that Eq. (6) which was used by Puls & Herrero (1988) to estimate the limits given in relation (7) is not valid in general. For the full multiline NLTE problem with changing continuum opacities, as is the case in realistic models, the line source function S_L depends nonlinearly on the radiation field $\overline{J}$. However, when the occupation numbers of the lower levels have stabilized, the linearity given in Eq. (6) holds approximately. Therefore we will compare and discuss different ALOs with respect to relation (7). Generally, a *divergent* behaviour can be expected for a region where

1. the ALO overestimates $diag(\underline{\underline{\Lambda}}')$ and
2. the rates are dominated by radiative line transitions.

2.2. Convergence problems with the Core Fraction Operator

The *Core Fraction Operator* was developed by Hamann (1985) and successfully applied for line transfer problems in WR-stars (for a recent review, see Hamann et al. 1991). However, for the unified models of O stars we encountered the difficulties described above since radiative rates dominate from the subsonic region on outwards.

Hamann's operator removes the physical reason for the failure of the Λ-iteration, namely the photons which are trapped in the optically thick line core. In order to accomplish this, he introduces a parameter γ (of order unity) which separates the optically thick core from the optically thin wings. Thus, a photon is said to belong to the line core if the optical depth τ_ν in any direction exceedes the value of γ.

Further, core saturation is assumed (Rybicki 1971), thus setting $\Lambda^*_\nu \equiv 1$ for the core frequencies and $\Lambda^*_\nu \equiv 0$ for the wings. Frequency integration leads to the core fraction f_c at every depth point:

$$\Lambda^* = f_c := \int_{\nu_{red}}^{\nu_{blue}} \varphi_\nu d\nu \tag{8}$$

where ν_{blue} and ν_{red} are the borders between line core and wings (depending on $v(r)$ and r) and calculated in a *Sobolev-type* solution as a function of γ.

With the expansion of the atomic model from 5/5/10 hydrogenic NLTE levels for the ions H I/He I/He II to 10/28/10 levels, and a realistic He I-structure, the core fraction operator failed to achieve convergence. The cause for this failure is demonstrated in Fig. 1, 2 and 3. While it is possible to choose an adequate value of γ so that Λ^* fulfills relation (7) for all strong and intermediate lines (Fig. 1 and 2), this is no longer possible for very weak lines (Fig. 3) and the crude overestimate of the exact diagonal in an area where radiative rates dominate leads to divergence. A drastic increase of γ would remove this divergence but then the well known problems of the Λ-iteration would occur.

The same behaviour can be observed in some figures published by Hamann (1985, see his Sect. 4: Fig. 3, 4 and 6) where the convergence rates are shown for an intermediate, a strong and a very strong line ($\kappa_0 = 10, 10^3$ and 10^5) and different values of γ. The strongest line converges slowly, but for *any* given value of γ, since $f_c(\gamma)$ underestimates $diag(\Lambda'_{\rm CMF})$ in all cases (compare Fig. 1). The intermediate line converges faster, because f_c is a better approximation to the exact diagonal, but diverges suddenly when γ falls below a critical value and f_c consequently overestimates $diag(\Lambda'_{\rm CMF})$ (compare Fig. 2).

There are several reasons for the mismatch between f_c and $diag(\Lambda'_{\rm CMF})$. First the discontinuous distinction between line core ($\Lambda^*_\nu \equiv 1$) and line wing ($\Lambda^*_\nu \equiv 0$) leads to a steeper gradient of f_c compared to $diag(\Lambda'_{\rm CMF})$. Further, the Sobolev Approximation used to calculate the integration boundaries, ν_{blue} and ν_{red}, breaks down around the sonic point. And finally, the continuum opacity is not taken into account, therefore f_c is not decreasing in the inner photosphere as the exact diagonal of $\Lambda'_{\rm CMF}$ does.

The problems with the core fraction operator f_c described above require the construction of an alternative ALO which satisfies the relation (7). Several possibilities are discussed in the following subsections.

2.3. Construction of an ALO for the CMF transport using the Sobolev Approximation

In this subsection we try to approximate $diag(\Lambda'_{\rm CMF})$ by the "diagonal" of the numerically very cheap Sobolev line transfer.

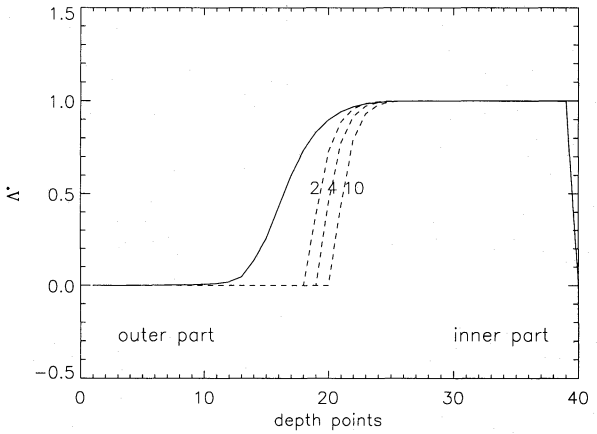

Fig. 1. Case of a strong line (Lyman α): Core fraction f_c (dashed lines) vs. depth point index for $\gamma = 2, 4$ and 10. For comparison, the exact diagonal of the CMF transport operator is shown (solid). The thermal point of H (see Sect. 3) is at depth point 22, the depth point index decreases with the radius

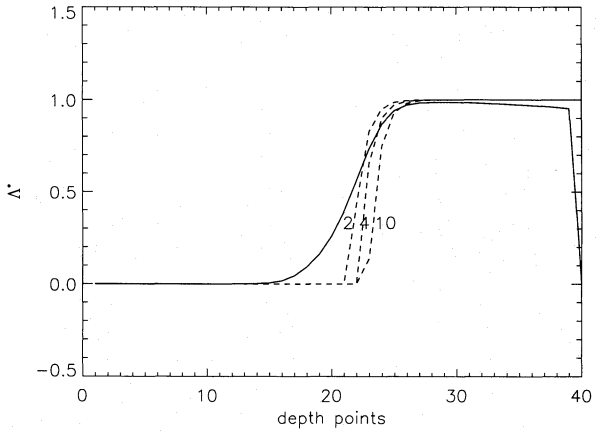

Fig. 2. Line of intermediate strength (Hγ): Core fraction f_c (dashed lines) and exact CMF diagonal (solid). Rest as Fig. 1

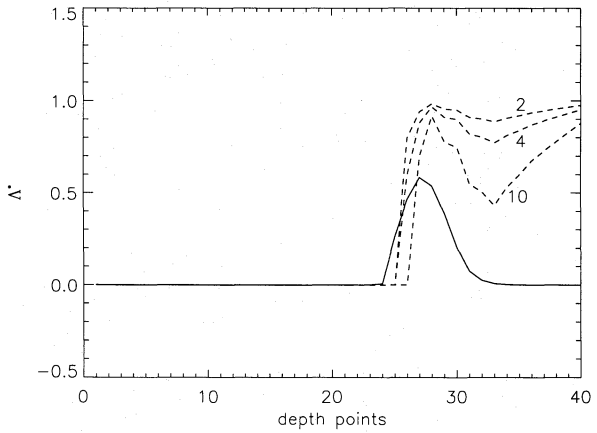

Fig. 3. Case of a weak line (He I 4471): Core fraction f_c (dashed lines) and exact CMF diagonal (solid); The thermal point of helium is here at depth point 23. Rest as Fig. 1

The usual Sobolev Approximation (SOB) yields for the mean line intensity

$$\overline{J}_{\rm SOB} = \beta_c I_c + (1-\beta) S^L \tag{9}$$

(β and β_c are the usual local escape probabilities given in Eq. (25) and I_c is the incident continuum intensity calculated from the emergent continuum flux at the line frequency; see for instance Paper I or Puls 1991). By comparison with Eq. (5), we may define the "diagonal" of the Sobolev line transfer as

$$diag(\Lambda'_{\rm SOB}) = 1 - \beta. \tag{10}$$

From Fig. 4, 5 and 6 we find that $(1-\beta)$ overestimates $diag(\Lambda'_{\rm CMF})$ in all cases of line strengths and therefore cannot be used as an ALO for CMF line transfer [3].

Almost the same behaviour is found using the improved Sobolev Approximation with continuum (SAC) developed by Hummer & Rybicki (1985). Following the notation of Puls & Hummer (1988), the mean line intensity in this case is given by

$$\overline{J}_{\rm SAC} = \overline{\beta_c I_c} + \overline{U} S_C + (1 - \beta - \overline{U}) S_L. \tag{11}$$

$\overline{\beta_c I_c}$ takes into account the actual intensity irradiating the resonance zone, S_C is the continuum source function and $\overline{U}$ gives the contribution of the *local* continuum inside the resonance zone. Hence, the "diagonal" of the Sobolev line transfer with continuum, i.e. the local contribution of S_L to $\overline{J}_{\rm SAC}$, is

$$diag(\Lambda'_{\rm SAC}) = 1 - \beta - \overline{U}\,. \tag{12}$$

Although the run of $(1-\beta-\overline{U})$ is now corrected concerning the contribution of the continuum opacity, the diagonal of the CMF transfer, $diag(\Lambda'_{\rm CMF})$, is still overestimated around the sonic point (Figs. 4 to 6, cf. also Puls 1991, Figs. 1 and 2). Therefore, also this operator is useless as an ALO *for the CMF transport*.

The difference between the diagonals of $\Lambda'_{\rm CMF}$ and $\Lambda'_{\rm SOB}$ or $\Lambda'_{\rm SAC}$ is not only caused by the breakdown of the Sobolev Approximation around the sonic point. In addition, $(1-\beta)$ and $(1-\beta-\overline{U})$ contain the contributions of the local line source function *integrated over the whole resonance zone*, whereas $diag(\Lambda'_{\rm CMF})$ is the *contribution of only one depth point* which decreases as the number of depth points is increased.

2.4. The CMF-Diagonal Operator

The best local ALO for CMF transport in unified atmospheres we found is the approximated diagonal constructed by Puls (1991), which we will call CMF-*Diagonal Operator*. The advantage of this operator is that – in all considered cases – it *never overestimates* the exact diagonal (see Figs. 4 to 6, dashed lines with crosses). Moreover, it is a very good approximation to the

[3] The use of $\Lambda^* = 1 - \beta$ to accelerate the line formation iteration within the *Sobolev Approximation* leads to good convergence rates and is in combination with the effective form of the rate equation (see Sect. 2.5) identical to the well known β, β_c iteration developed by Klein & Castor (1978) (cf. Puls 1991).

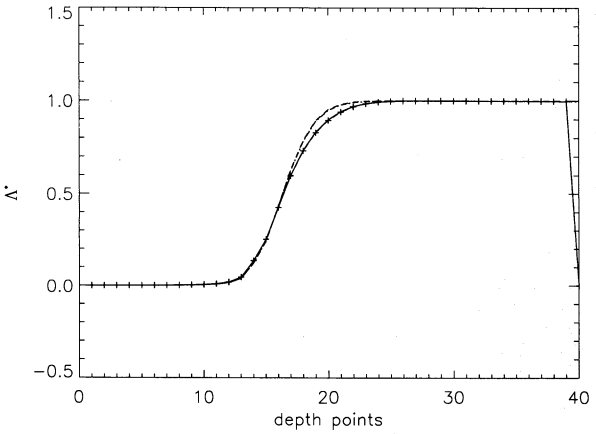

Fig. 4. Case of a strong line (Lyman α, as Fig. 1): The "diagonal" of the Sobolev transfer, $(1-\beta)$, (dashed), of the SAC transfer, $(1-\beta-\overline{U})$, (dashed dotted) and the approximated CMF-Diagonal Operator (dashed with crosses) compared to the exact CMF diagonal (solid)

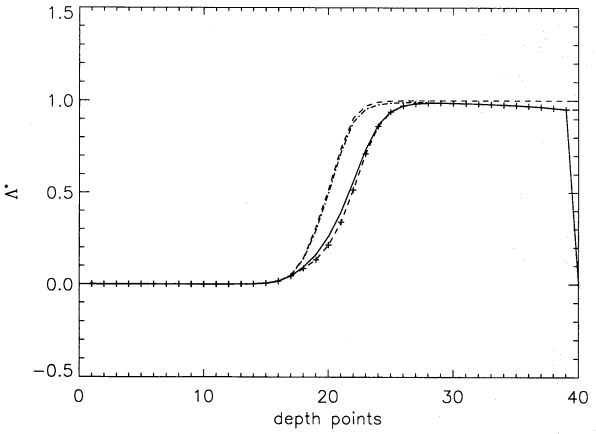

Fig. 5. Line of intermediate strength (Hγ): $(1-\beta)$ dashed, $(1-\beta-\overline{U})$ dashed dotted and approximated CMF-Diagonal Operator (dashed with crosses) compared to the exact CMF diagonal (solid)

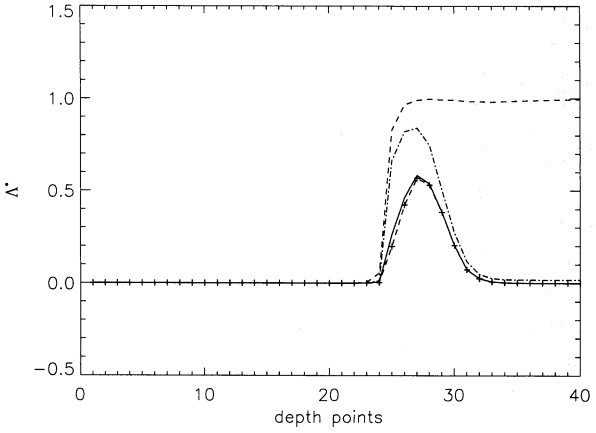

Fig. 6. Case of a weak line (He I 4471): $(1-\beta)$ dashed, $(1-\beta-\overline{U})$ dashed dotted and approximated CMF-Diagonal Operator (dashed with crosses) compared to the exact CMF diagonal (solid)

exact diagonal and can be calculated with a reasonable amount of computer time. This ALO leads to an extreme fast convergence for the line iteration problem, even when more than 600 line transitions are included (see Fig. 7).

The calculation of the CMF-Diagonal Operator has to be done in parallel with the CMF transport. We will give a somewhat different description of this calculation compared to Puls (1991) in order to clarify which terms are neglected when the exact diagonal is approximated. The transport equations for the Feautrier itensities u_ν and v_ν in the CMF are

$$\frac{\partial u_\nu}{\partial \tau_\nu} + \frac{\nu_0}{c}\cdot\left[\mu^2\frac{\mathrm{d}v}{\mathrm{d}r} + (1-\mu^2)\frac{v}{r}\right]\frac{1}{\chi_\nu}\cdot\frac{\partial v_\nu}{\partial \nu} = v_\nu \qquad (13)$$

$$\frac{\partial v_\nu}{\partial \tau_\nu} - \frac{\nu_0}{c}\cdot\left[\mu^2\frac{\mathrm{d}v}{\mathrm{d}r} + (1-\mu^2)\frac{v}{r}\right]\frac{1}{\chi_\nu}\cdot\frac{\partial u_\nu}{\partial \nu} = u_\nu - S_\nu \qquad (14)$$

(cf. Mihalas 1978, pp 499). After discretization (*ND* depth points labelld with indices i, l and *NF* frequency points labelled with index k) and reformulation these equations yield

$$\sum_{i=l-1}^{l+1}(T_k)_{li}\,u_{k\,i} = U_{ki}\,u_{k-1\,l} - VA_{kl}\,v_{k-1\,l-\frac{1}{2}} + VB_{kl}\,v_{k-1\,l+\frac{1}{2}} + (1-\rho_{kl})S_{Cl} + \rho_{kl}\,S_{Ll} \qquad (15)$$

$$v_{k\,l-\frac{1}{2}} = G_{k\,l-\frac{1}{2}}(u_{k\,l} - u_{k\,l-1}) + H_{k\,l-\frac{1}{2}}\,v_{k-1\,l-\frac{1}{2}} \qquad (16)$$

The indices $(l \pm \frac{1}{2})$ correspond to quantities defined on depth point interstices. $\underline{\underline{T}}_k$ is a *tridiagonal* matrix which additionally has *diagonal dominance*, a fact which simplifies the solution algorithm. The definition of all matrix elements and coefficients of Eqs. (15) and (16) as well as the solution algorithm and the boundary conditions are given and discussed in Mihalas (1978, pp 505). In monotonically expanding atmospheres the line radiation field is only influenced by continuum radiation of higher frequencies (if no line overlap present), thus the system of equations (15) and (16) can be solved from the blue side, with decreasing frequencies for increasing index k and with the blue wing boundary conditions $\underline{u}_1 = \underline{u}_C$ and $\underline{v}_1 = \underline{v}_C$ (the index C denotes continuum intensities).

If the continuum opacities are kept fixed, the CMF transport equation has the quasi affine form given in Eq. (5) (insert Eq. (16) for (k-1) into (15) and integrate the resulting u_ν weighted with φ_ν over frequency ν and angle cosine μ). The influence of the continuum, i.e. S_C and the boundary conditions for u_1 and v_1, passes linearly through the system of equations (15) and (16) for $k = 1 \ldots NF$ and is responsible for the displacement vector $\underline{\Phi}$. However, as the factors $\rho_{k\,l}$ can change slightly during the line iteration, $\underline{\Phi}$ is only approximately constant.

Keeping in mind that we want to find the diagonal of the linear contribution to Λ, i.e. $diag(\underline{\underline{\Lambda}}')$ (see Eq. (5)), we define a corresponding primed Feautrier intensity u'_ν by

$$\Lambda'[S_L] =: \overline{J}' =: \int_0^1\int_0^\infty u'_\nu\,\varphi_\nu\,d\nu\,d\mu \qquad (17)$$

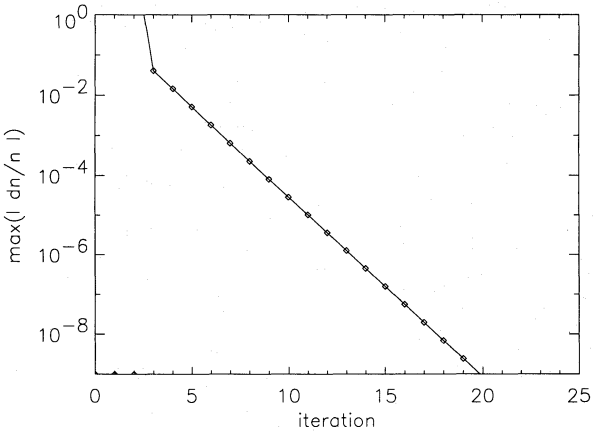

Fig. 7. Convergence of line transfer for the CMF-Diagonal Operator: The maximum absolute values of the relative corrections for the occupation numbers are shown

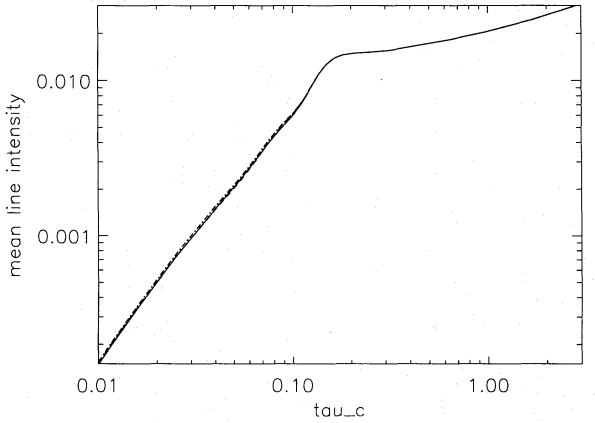

Fig. 8. Case of a strong line (Lyman α): The mean line intensity $\overline{J}$ in cgs vs. continuum optical depth τ_c is shown for three cases, namely CMF (solid), SAC (dashed dotted) and SOB (dashed)

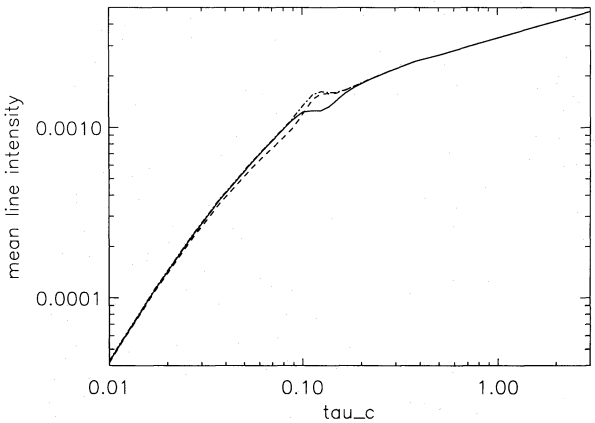

Fig. 9. Line of intermediate strength (Hγ): $\overline{J}$ in cgs vs. τ_c for CMF (solid), SAC (dashed dotted) and SOB (dashed). The local maximum of $\overline{J}_{\rm SOB}$ and $\overline{J}_{\rm SAC}$ is due to the maximum of dv/dr (Fig. 11)

and v'_ν analogously where μ is the cosine of the angle between the ray and the radius vector. The so-defined $u'_{k\,l}$ and $v'_{k\,l}$ represent the linear contribution to Λ and are calculated as $u_{k\,l}$ and $v_{k\,l}$ from Eqs. (15) and (16) but with the boundary conditions $u'_{1\,l} = v'_{1\,l} = 0$ and $S_{C\,l} = 0$.

Provided that the coefficients $\rho_{k\,l}$ remain constant during the line iteration, it is possible to write $u'_{k\,l}$ and $v'_{k\,l}$ in terms of the line source function $S_{L\,j}$:

$$u'_{k\,l} =: \sum_j f^j_{k\,l} \cdot S_{Lj} \qquad \text{and} \qquad v'_{k\,l\pm\frac{1}{2}} =: \sum_j g^j_{k\,l\pm\frac{1}{2}} \cdot S_{Lj} \quad (18)$$

(the indices j, l account for depth points, the index k for frequency points). The coefficients $f^j_{k\,l}$ are the fractional contributions of S_{Lj} to $u'_{k\,l}$ which are responsible for the linear part of the line radiation transport. The diagonal elements of $\underline{\underline{\Lambda}}'$ can be constructed from these coefficients, taking into consideration the frequency- and angle-integration. The angle-integration is replaced by an integration over the impact parameter p (since pz-geometry is used), thus we find

$$\Lambda^*_{ll} := \Lambda'_{ll} = \sum_{jp} w_{jp} \sum_k w_k \varphi_k f^l_{k\,l} \quad (19)$$

where w_{jp} and w_k are integration weights for impact parameter p and comoving frame frequency ν.

The exact CMF diagonal can be found once the *diagonal* coefficients $f^l_{k\,l}$ have been determined. Since the influence of S_L passes linearly through Eqs. (15) and (16), one can calculate the coefficients $f^j_{k\,l}$ in the same way as $u'_{k\,l}$, however, replacing S_{Li} by the Kronecker symbol δ_{ij}, $u'_{k-1\,i}$ by $f^j_{k-1\,i}$ and $v'_{k-1\,i\pm\frac{1}{2}}$ by $g^j_{k-1\,i\pm\frac{1}{2}}$ together with boundary conditions as for the calculation of the primed Feautrier variables:

$$\begin{aligned} f^j_{k\,l} &= \sum_i (T^{-1}_k)_{li} \Big[U_{ki}\, f^j_{k-1\,i} - VA_{ki}\, g^j_{k-1\,i-\frac{1}{2}} \\ &\quad + VB_{ki}\, g^j_{k-1\,i+\frac{1}{2}} + \delta_{il}\, \rho_{ki} \Big] \\ g^j_{k\,l-\frac{1}{2}} &= G_{k\,l-\frac{1}{2}} (f^j_{k\,l} - f^j_{k\,l-1}) + H_{k\,l-\frac{1}{2}}\, g^j_{k-1\,l-\frac{1}{2}} \\ g^j_{k\,l+\frac{1}{2}} &= G_{k\,l+\frac{1}{2}} (f^j_{k\,l+1} - f^j_{k\,l}) + H_{k\,l+\frac{1}{2}}\, g^j_{k-1\,l+\frac{1}{2}} \,. \end{aligned} \quad (20)$$

The boundary conditions are

$$f^j_{1\,l} = 0 \qquad \text{and} \qquad g^j_{1\,l\pm\frac{1}{2}} = 0 \qquad (j, l = 1..ND).$$

According to (20) the calculation of the exact diagonal requires the inversion of the $ND \times ND$ matrix $\underline{\underline{T}}_k$ which is equivalent to the complete determination of $\underline{\underline{\Lambda}}'$. Thus, we would lose the advantage of the iteration-scheme compared with the direct solution of Eqs. (15), (16). Since $\underline{\underline{T}}^{-1}_k$ is a full matrix, the full summation in Eq. (20) would also have to be carried out and all off-diagonal coefficients $f^l_{k-1\,i}$ ($i = 1...ND$) would have to be calculated to obtain the *exact* coefficients $f^l_{k\,l}$.

Fortunately, $\underline{\underline{T}}_k$ and therefore also $\underline{\underline{T}}^{-1}_k$ are almost diagonal, so it is possible to approximate Eqs. (20). Since $|(T^{-1}_k)_{ll}| \gg$

$|(T_k^{-1})_{li}|$ $(i \neq l)$, the off-diagonals $f^l_{k\,i}$ $(i \neq l)$ can be neglected and one can *approximate* contributions to the diagonal of $\underline{\underline{\Lambda}}'$ by

$$\begin{aligned} f^l_{k\,l} &\approx (T_k^{-1})_{ll}\Big[U_{kl}\, f^l_{k-1\,l} - VA_{kl}\, g^l_{k-1\,l-\frac{1}{2}} \\ &\quad + VB_{kl}\, g^l_{k-1\,l+\frac{1}{2}} + \rho_{kl}\Big] \\ g^l_{k\,l-\frac{1}{2}} &\approx G_{k\,l-\frac{1}{2}}\, f^l_{k\,l} + H_{k\,l-\frac{1}{2}}\, g^l_{k-1\,l-\frac{1}{2}} \\ g^l_{k\,l+\frac{1}{2}} &\approx -G_{k\,l+\frac{1}{2}}\, f^l_{k\,l} + H_{k\,l+\frac{1}{2}}\, g^l_{k-1\,l+\frac{1}{2}}\,. \end{aligned} \tag{21}$$

The diagonal elements $(T_k^{-1})_{ll}$ of the inverse of a tridiagonal matrix can be calculated quickly with a procedure developed by Rybicki & Hummer (1990) and the other matrix elements are given anyway. Summation according to Eq. (19) gives the CMF-Diagonal Operator.

Two comments should be given here:

1. In contrast to the Sobolev "diagonal", the CMF diagonal containes *only the contribution of one depth point* and therefore approaches zero with increasing number of depth points which *can reduce the success of the Accelerated Lambda Iteration*. The other way around, however, the convergence rate can be enhanced significantly with a lower number of grid points (cf. Olson et al. 1986).
2. Before the CMF-Diagonal Operator had been developed, we applied the method of *full rates with acceleration term* (Pauldrach & Herrero 1987; Gabler et al. 1989) to overcome the convergence problems as described above. This technique avoids the appearence of negative (effective) rates, the cause of a divergent behavior; however, it results in an oscillating convergence pattern due to the fact that the *acceleration term* has to be approximated by the value of the previous iteration. In contrast, the use of our CMF-Diagonal Operator no longer causes any problems connected with the direct use of the *effective rates*, simply because the differences $(\Lambda[S_L^{n-1}] - \Lambda^* \cdot S_L^{n-1})$ cannot become negative.

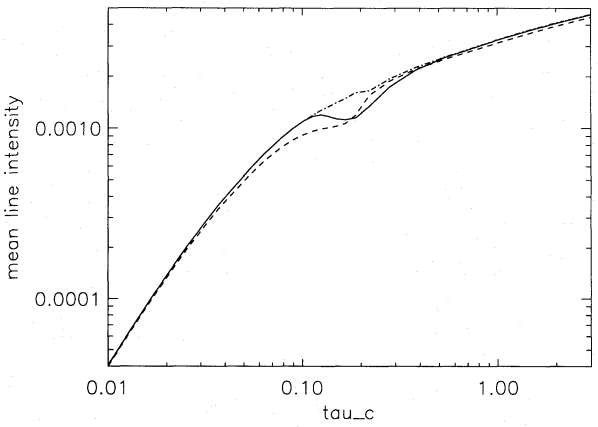

Fig. 10. Case of a weak line (He I 4471): $\overline{J}$ in cgs vs. τ_c for CMF (solid), SAC (dashed dotted) and SOB (dashed). The local minimum of $\overline{J}_{\rm CMF}$ is explained in the text

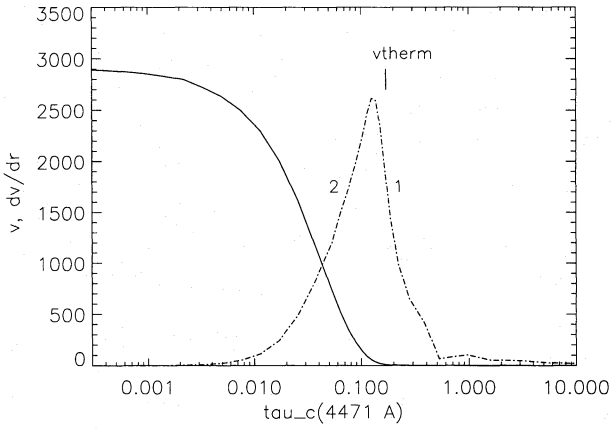

Fig. 11. Velocity field in km/s (solid) and velocity gradient in cgs multiplied by 10^7 (dashed dotted) for the same model as in Figs. 1 to 13 versus the continuum optical depth at He I 4471. "vtherm" indicates the point where the wind reaches the thermal velocity of He, the numbers "1" and "2" indicate zones with a rapidly changing velocity gradient

3. Line formation through the thermal point

As we will show later, most of the optical H and He profils of O stars are strongly affected by the region around the thermal point, i.e. the point where the velocity field reaches $v_{\rm therm}$, the thermal velocity of the ion. Unfortunately the radiation transport in this region is difficult to handle, since important quantities such as the velocity gradient are changing rapidly. Hence, the commonly used Sobolev Approximation becomes inapplicabel as it is based on a constant velocity gradient $\mathrm{d}v/\mathrm{d}r$ throughout the whole resonance zone. Nevertheless, an *accurate* radiation transfer at the thermal point is *crucial* for line formation in O stars since the radiative rates dominate from the subsonic part on.

In this section we discuss the differences between the (numerically very cheap) pure Sobolev transport (SOB), the improved Sobolev Approach with Continuum (SAC) and the (very time consuming) CMF transfer and show the consequences on the calculated profiles. The SOB and SAC transport equations are given by Eqs. (9) and (11), a reference for the solution of the CMF transfer can be found in Sect. 2.4. The solution in the CMF can be regarded as exact in monotonically expanding atmospheres.

In order to demonstrate the effects on the radiation field, we calculate the mean line intensity $\overline{J}$ (which couples radiation transfer and rate equations) as a result of SOB, SAC and CMF line transfer, *using the occupation numbers from a converged CMF model*. For a strong line all three methods have nearly identical results (Fig. 8). For intermediate and weak lines (Figs. 9 and 10), the CMF solution shows a local minimum just at the thermal point, which is not present in the SAC calculations. This local minimum is more pronounced for weaker lines. The SOB results differ in a larger region around the thermal point (see Figs. 9, 10 and 12) mainly because the angular distribution of the continuum intensity is not considered which is treated more

accurately in the SAC case (see Hummer & Rybicki 1984; Puls & Hummer 1987).

The general argument for the failure of the Sobolev transfer is that the concept of a local resonance zone with constant opacity, emissivity and velocity gradient is not valid in the subthermal region. In consequence one would expect also the SAC transfer to fail in the complete region with $v \leq v_{\rm therm}$. However, deep enough in the atmosphere the escape probabilities are small ($\beta \approx \beta_c \approx 0$) and the photons are contributed by local conditions. Consequently we have $\overline{J} \approx S_\nu$ independent of the approximation used. This explains why $\overline{J}_{\rm SAC}$ deviates from $\overline{J}_{\rm CMF}$ only in a distinct area around the sonic point. The same argument can be used to explain why stronger lines are less affected: The lines are still optically thick at the sonic point ($\beta \approx 0$) hence the mean line intensity is identical to the line source function, i.e. $\overline{J}_{\rm SAC} \approx \overline{J}_{\rm CMF} \approx S_L$.

The local minimum of $\overline{J}_{\rm CMF}$ around the thermal point is an effect of the rapid change in the velocity gradient (Fig. 11), i.e. of the curved velocity field, which leads to an asymmetric situation for outward and inward directed photons in a sense that photons propagating from inside towards the thermal point are absorbed more effectively than photons coming from outside (a more detailed explanation is given in the Appendix).

The above discussion concerning the accuracy in $\overline{J}$ by the different methods is especially important from the point of view that the quantities determining the occupation numbers are in principle the net radiative rates:

$$Z_{ji} = 1 - \overline{J}/S_L. \qquad (22)$$

As $\overline{J}$ and S_L have similar values, the difference of $\overline{J}/S_L$ from unity is much more uncertain than $\overline{J}$ itself (Fig. 12). This difference leads to erroneous occupation numbers as long as the radiative rates dominate, *which is the case for O and Of stars* in the line forming regions.

The effect of this difference in $\overline{J}$ on the line source function S_L in two *independently converged* CMF and SAC models is shown in Fig. 13. Peforming the formal integral in the observers frame yield emergent flux profiles which differ by up to 15% in aequivalent width for a weak line (Fig. 14).

Additionally, the errors made in $\overline{J}_{\rm SAC}$ for weak and intermediate lines also influence the lower and the upper occupation numbers of strong lines. In consequence the calculated profiles of strong observeable lines like Hα and He II 4686 are also affected when SAC transfer is used (Figs. 15 and 16), even though $\overline{J}_{\rm SAC}$ being almost correct for those lines. Since similar effects were found for all our O and Of-star models, we conclude that the line formation (for optical H and He lines) has to be calculated in the comoving frame.[4]

[4] A mixed treatment, SAC for strong lines and CMF for the remaining lines, is in principle possible. This can save some amount of computational time when metal lines are included. For H and He line formation, however, the number of strong lines which can be treated with SAC transfer is negligible, so that a general CMF transfer was performed.

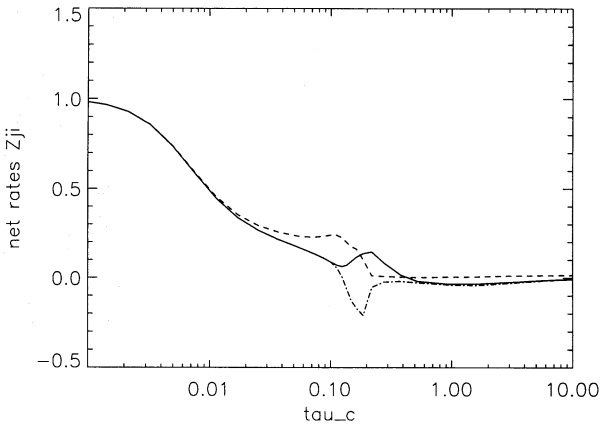

Fig. 12. Net radiative rates Z_{ji} for He I 4471 in case of CMF transfer (solid), SAC (dashed dotted) and SOB (dashed); same line and model as Fig. 10

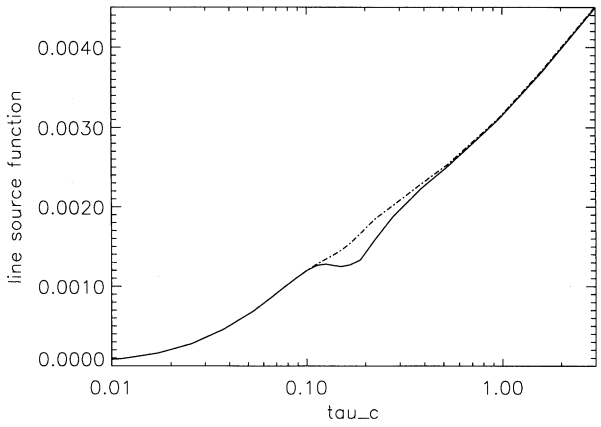

Fig. 13. Line source function S_L in cgs for He I 4471 for two models converged separately by using CMF (solid) and SAC (dashed dotted) transport

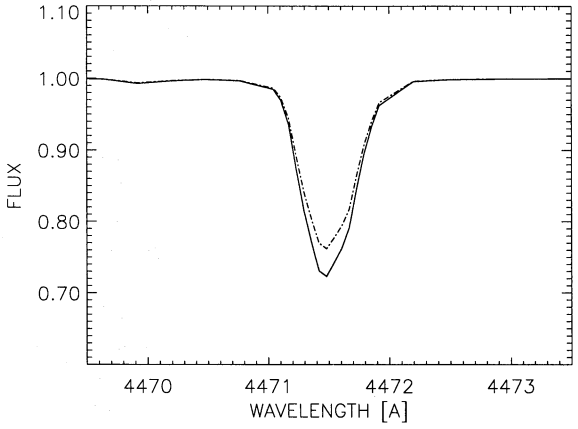

Fig. 14. He I 4471 profile based on S_L shown in Fig. 13 for CMF (solid) and SAC (dashed dotted). The bump in the blue wing is due to a forbidden component

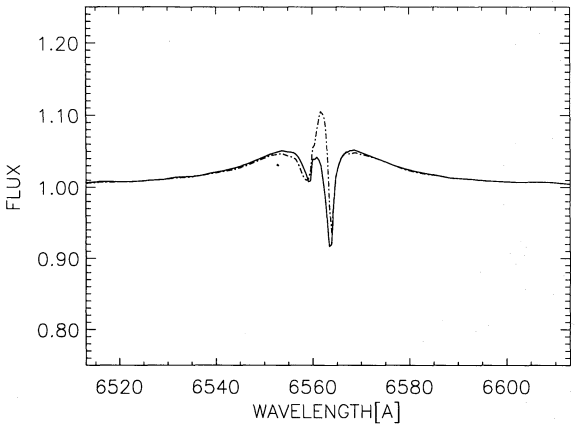

Fig. 15. Hα profile for CMF (solid) and SAC (dashed dotted). The blue shifted absorption component is due to the blend with the He II 4/6 line

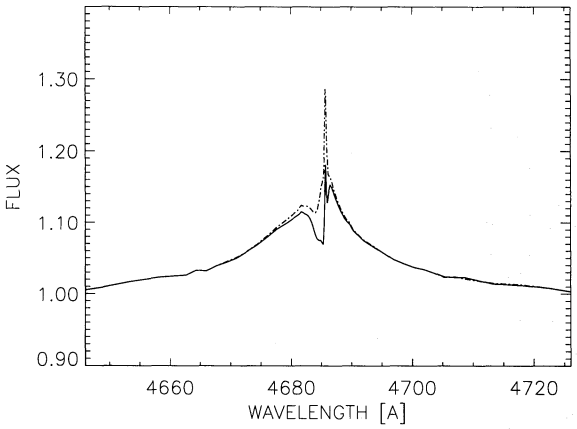

Fig. 16. He II 4686 profile for CMF (solid) and SAC (dashed dotted)

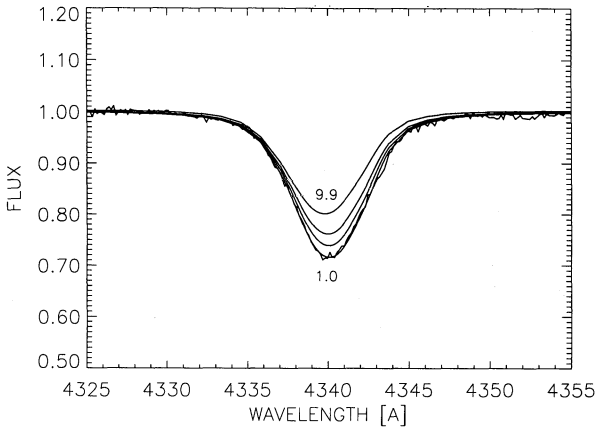

Fig. 17. Observed and calculated Hγ profiles of ζ Puppis; The calculated profiles are rotationally broadend with $v \cdot \sin i$ = 200 km/s. As stellar parameters we adopted $T_{\rm eff}$ = 42 000 K, $\log g$ = 3.5, $R/R_\odot$ = 18 and N_{He}/N_H = 0.16 together with a sequence of $\dot{M}$ = 1.0, 3.2, 5.5 and 9.9 $\cdot\, 10^{-6} M_\odot$/yr

4. Wind contamination of H and He profiles

The calculations in Paper I have already shown that "photospheric" absorption lines such as Hγ are affected by the emission of the surrounding stellar wind. It was concluded that this could have consequences for the determination of stellar parameters from the analysis of photospheric lines using the standard plane parallel hydrostatic models. A further investigation of this point was, however, hampered by the convergence problems with the old "core fraction" CMF line transfer. With our new technique, the accurate calculation of wind contaminated line profiles is straight forward.

As a first step, we have therefore studied the case of two early type supergiants, Melnick 42 and ζ Puppis. We intend to demonstrate that the wind contamination effect of Hγ is significant and will require a complete reanalysis of these objects by means of unified models. For this purpose, we use the stellar parameters obtained from the standard analysis with plane parallel hydrostatic models and calculate sequences of unified models, where the radiative line force multiplier parameters k, α (see Paper I) are varied so that the same terminal velocities (as observed) but different mass loss rates are obtained (for details see also Gabler et al. 1990). In this way the gradual increase of the wind contamination as function of mass loss rate can be studied.

We start with the galactic O4f-star ζ Puppis. According to Kudritzki et al. (1983), Bohannan et al. (1986), Voels et al. (1989) it has an effective temperature of about 42 000 K, a gravity of $\log g$= 3.5, an enhanced helium abundance $N_{\rm He}/N_{\rm H}$ of 0.16 to 0.20 and a stellar radius R_* = 18$R_\odot$. From the radio flux and the Hα emission the mass loss rate is estimated to be in the range of 3 to 5 $\cdot 10^{-6} M_\odot$/yr (see for instance Kudritzki et al. 1992).

In Fig. 17 we show the observed Hγ line profile (published in Bohannan et al. 1990) compared with a sequence of unified models with different mass loss rates. The effect of wind contamination can be clearly seen as it fills up the absorption profile with increasing mass loss. Only the model with the unrealistically low mass loss rate fits the observation since the parameters $T_{\rm eff}$ and $\log g$ were gained assuming $\dot{M}$= 0. To fit the observed profile with $\dot{M}$= 3 to 5 $\cdot 10^{-6} M_\odot$/yr would require an enhancement of the gravity by 0.10 to 0.15 dex.

The second example is the O3f/WN-star Melnick 42 in the LMC. This object was a target in the HST science verification phase and was therefore studied by Heap et al. (1991). From the "hydrostatic" analysis of the optical "photospheric" lines they found $T_{\rm eff}$= 42 500 K , $\log g$= 3.5, $R/R_\odot$ = 28 and a normal helium abundance. From the analysis of the UV-lines they determined a metal abundance of roughly 1/4 solar, a terminal velocity of 3 000 km/s and $\dot{M}$= 4 $\cdot 10^{-6} M_\odot$/yr. However, they noted that the value for $\dot{M}$ was highly uncertain.

Because of this uncertainty, we first used the sequence of unified models to (roughly) determine the mass loss rate from the strong Hα and He II 4686 emission of this object. This is done in Figs. 18 and 19. We conclude that the mass loss rate should be in the range of 10 to 20 $\cdot 10^{-6} M_\odot$/yr, much higher

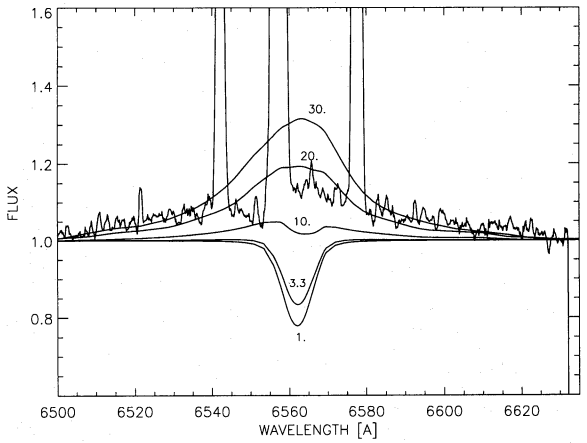

Fig. 18. Observed and calculated Hα-profile of Melnick 42: The calculated profiles are rotationally broadend with $v \cdot \sin i$ = 240 km/s. The adopted stellar parameters are $T_{\rm eff}$ = 42 500 K, $\log g$ = 3.5, $R/R_\odot$ = 28 and N_{He}/N_H = 0.1, the adopted mass loss rates are 1.0, 3.3, 10, 20, and 30 $\cdot 10^{-6} M_\odot$/yr. Observation by Voels using the ESO 3.6 m telescope and the CASPEC spectrograph. Note the central emission of the surrounding H II region in the line center and several other emission peaks caused by cosmic events during the long exposures

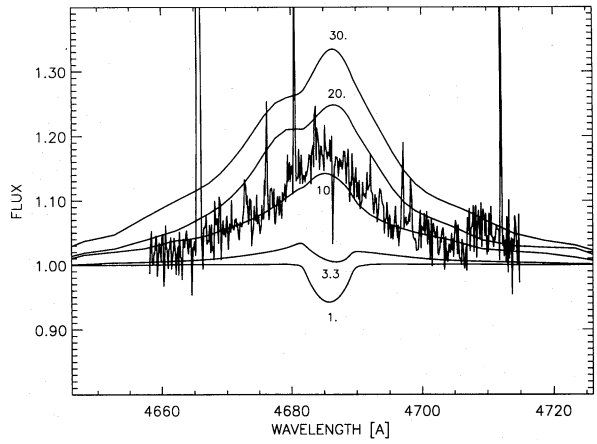

Fig. 19. He II 4686 of Melnick 42; adopted parameters as in Fig. 18, $\dot{M}$ indicated in units of $10^{-6} M_\odot$/yr

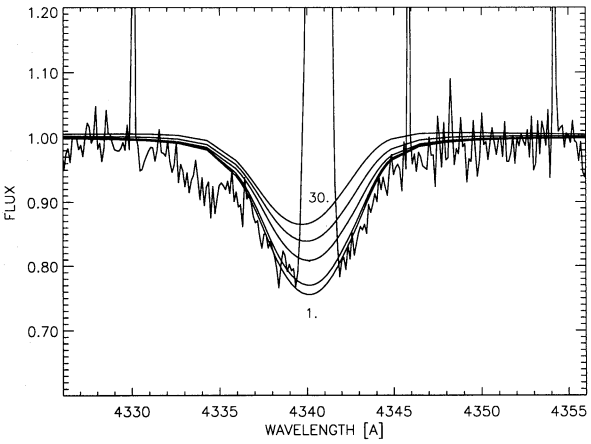

Fig. 20. Hγ of Melnick 42; adopted parameters as in Fig. 18, $\dot{M}$ indicated in units of $10^{-6} M_\odot$/yr

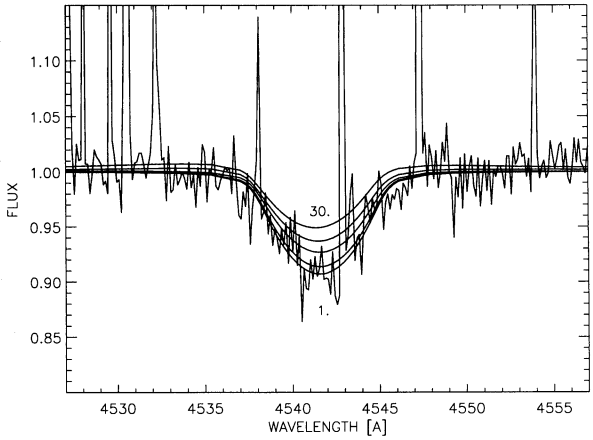

Fig. 21. He II 4542 of Melnick 42; adopted parameters as in Fig. 18, $\dot{M}$ indicated in units of $10^{-6} M_\odot$/yr

than found by Heap et al. Then we calculated Hγ and He II 4542 line profiles to study the effects of wind contamination (Figs. 20 and 21). It is obvious that for the values of $\dot{M}$ obtained from Hα and He II 4686 the contamination effect is severe. In consequence, the stellar parameters obtained by means of hydrostatic NLTE calculations for the optical hydrogen and helium lines must be regarded as extremly uncertain.

We conclude that for OB-supergiants with strong mass loss a complete reanalysis by means of unified models for the determination of stellar parameters will be needed. This work has now been started and results will be forthcoming soon.

Future improvements are necessary concerning the treatment of line blocking. Test calculations showed that this effect can influence the ionization structure and consequently the value of $\dot{M}$ concluded from the emission lines.

Acknowledgements. Many thanks to David Hummer, Stan Owocki and Wolf-Rainer Hamann for helpful discussions and critical comments. We also thank Gudrun Taresch for providing routines for the SAC line transfer. This work was supported by the Deutsche Forschungsgemeinschaft under grant Ku 474/16-1 and by the BMFT under grant 010R9008.

Appendix: a 2nd order Sobolev approximation

In general, a 2nd order Sobolev theory has to account for the gradients of the line source function and the opacity and the curvature of the velocity field (cf. Eqs. 9, 23 and 25). In this Appendix we concentrate on the implications of the curved velocity field which is primarily responsible for the break down of the first order Sobolev Approximation at the thermal point (compare Sect. 3).

The first order Sobolev Approximation (Eqs. 9 and 11) is usually applied to rapidly expanding atmospheres and uses the concept of a *local* resonance zone, where a photon with given observer's frame frequency $\nu_{\rm OF}$ can interact with line absorption/emission of the moving medium (Sobolev 1957; for a more recent description see Rybicki & Hummer 1978). Quantities like the velocity gradient $\mathrm{d}v/\mathrm{d}r$, the line source function S_L and the line opacity χ^L are assumed to be constant over the whole resonance zone of a line. The optical thickness of this interaction zone is then

$$\begin{aligned}\tau_{\rm S}(r,\mu) &= \chi^L(r)\frac{c}{\nu_0}\left[\left.\frac{\partial(\mu v)}{\partial z}\right|_p(z_0)\right]^{-1} \\ &= \chi^L(r)\frac{c}{\nu_0}\left[\mu^2\frac{\mathrm{d}v}{\mathrm{d}r}+(1-\mu^2)\frac{v}{r}\right]^{-1}\end{aligned} \tag{23}$$

where (in p-z geometry) the pair (r,μ) is related to (p,z_0) by

$$r^2 = p^2 + z_0^2 \quad \text{and} \quad \mu = \pm\sqrt{1-(p/z_0)^2}. \tag{24}$$

χ^L is the line opacity coefficient, c the speed of light, ν_0 the line frequency and $\left(\partial(\mu v)/\partial z|_p(z_0)\right)$ the partial derivative of the projected velocity for fixed p at point z_0 (see Fig. 22a).

The escape probability for photons at radius r is then given by

$$\beta(r) = \frac{1}{2}\int_{-1}^{1}\frac{1-e^{-\tau_{\rm S}(r,\mu)}}{\tau_{\rm S}(r,\mu)}\mathrm{d}\mu\,. \tag{25}$$

The corresponding core escape probability β_c is calculated in the same way but with the lower integration boundary replaced by $\mu_c = \sqrt{1-(R_*/r)^2}$, the cosine of the angle subtended by the stellar core with radius R_*.

In contrast to the common assumption of constant $\mathrm{d}v/\mathrm{d}r$, the velocity gradient varies rapidly around the thermal point (see Sect. 3 and Fig. 11), which causes the Sobolev Approximation to become inapplicable. The effect of this velocity curvature on the line force is discussed in Owocki (1991) and Owocki & Zank (1991) in terms of a "Radiative Viscosity". In order to understand the influence of a non-constant $\partial(\mu v)/\partial z$ on the mean line intensity $\overline{J}$, we expand the projected velocity to second order around z_0

$$(\mu v)(z) \approx (\mu v)(z_0) + \left.\frac{\partial(\mu v)}{\partial z}\right|_p(z_0)\cdot l + \frac{1}{2}\left.\frac{\partial^2(\mu v)}{\partial z^2}\right|_p(z_0)\cdot l^2 \tag{26}$$

with $l = (z - z_0)$. The 2nd order term proportional to l^2 leads to a variable (optical) thickness of the resonance zone as function of the observer's frame frequency $\nu_{\rm OF}$ (compare Figs. 22a and 22b). The frequency dependent optical depth from the "inner" boundary of the resonance zone $z_{\rm min}$ to the considerd point z_0 is given by

$$\widetilde{\tau}_+(\nu_{\rm OF}) = \int_{z_{\rm min}(\nu_{\rm OF})}^{z_0}\chi^L\cdot\varphi\left[\nu_{\rm OF}-\frac{\nu_0}{c}\cdot(\mu v)(z)\right]\mathrm{d}z \quad (\mu \geq 0). \tag{27}$$

The corresponding optical depth $\widetilde{\tau}_-$ for $\mu < 0$ is calculated analogously from z_0 to the outer boundary $z_{\rm max}(\nu_{\rm OF})$. The boundaries $z_{\rm min}$ and $z_{\rm max}$ are functions of the frequency and defined by a vanishing profile function φ_ν in Eq. (27), i.e. when the CMF frequency $\nu_{\rm CMF}$ (see below) is shifted about 3 to 4 Doppler widths out of the line center ν_0. (The sum $\widetilde{\tau}_+ + \widetilde{\tau}_-$ is the total optical thickness of the interaction zone and corresponds to $\tau_{\rm S}$ defined in Eq. (23); Note that $\widetilde{\tau}_+(\nu \gg \nu_0) = \widetilde{\tau}_-(\nu \ll \nu_0) = 0$). For simplicity and to demonstrate the effects of the variable $\partial(\mu v)/\partial z$ only, we assume χ^L to be constant over the interaction zone as in first order Sobolev Approximation. Further, a Doppler profile (with a constant thermal velocity $v_{\rm therm}$ within the resonance zone) is assumed for φ and the observer's frame frequency $\nu_{\rm OF}$ is replaced by the CMF-frequency

$$\nu_{\rm CMF} \approx \nu_{\rm OF} - \frac{\nu_0}{c}(\mu v)(z_0). \tag{28}$$

If the expansion given in Eq. (26) is inserted into Eq. (27), one can calculate the optical depth from z_0 to the inner boundary of the resonance zone as

$$\widetilde{\tau}_+(r,\mu,\nu_{\rm CMF}) = \frac{\chi^L}{\nu_0}\cdot\frac{c}{v_{\rm therm}}\cdot\frac{1}{\sqrt{\pi}}\int_{l_{\rm min}}^{0}e^{-x_+^2(l)}\mathrm{d}l \quad \text{for } \mu \geq 0 \tag{29}$$

with $l_{\rm min} := z_{\rm min} - z_0$ (the integration variable l is here negative). The corresponding optical depth $\widetilde{\tau}_-$ from z_0 to the outer boundary for inward directed photons ($\mu < 0$) is calculated analogously to (29) but as integral of $\exp[-x_-^2(l)]$ from $l = 0$ to $l_{\rm max} := z_{\rm max} - z_0$. The dimensionless frequency variables x_+ and x_- in Eq. (29) are

$$\begin{aligned}x_\pm(l) &= \frac{1}{v_{\rm therm}}\cdot\left\{\frac{\nu_{\rm CMF}-\nu_0}{\nu_0}\cdot c \mp \left[(1-\mu^2)\frac{v}{r}+\mu^2\frac{\mathrm{d}v}{\mathrm{d}r}\right]\cdot l\right. \\ &\quad \left. -\frac{1}{2}\left[\mu^3\frac{\mathrm{d}^2v}{\mathrm{d}r^2}+3\mu\frac{1-\mu^2}{r}\left(\frac{\mathrm{d}v}{\mathrm{d}r}-\frac{v}{r}\right)\right]\cdot l^2\right\}\end{aligned} \tag{30}$$

for the both cases, $\mu < 0$ and $\mu \geq 0$. All quantities χ^L, μ, r, v, $\mathrm{d}v/\mathrm{d}r$, $\mathrm{d}^2v/\mathrm{d}r^2$ and the thermal velocity $v_{\rm therm}$ are taken at radius r which corresponds to the point z_0 indicated in Fig. 22b.

The difference between $\widetilde{\tau}_+$ and $\widetilde{\tau}_-$ is due to the different sign of μ in Eqs. (29) and (30). For the resonance frequency $\nu_{\rm CMF} = \nu_0$ we see immediately that the 2nd order term in Eq. (30) causes $\widetilde{\tau}_+$ and $\widetilde{\tau}_-$ to be different. Neglecting this term we would obtain $\tau_+ = \tau_- = \tau_S/2$ at $\nu_{\rm CMF} = \nu_0$.

In order to develope a transport equation we use the same simplifications which were made for the first order Sobolev Approximation: It is assumed that the non local contribution to $\overline{J}$, i.e. $\beta_c I_c$ in Eq. (9), is not modified by continous absorption and further that the local contribution is dominated by the line source function S_L which is also assumed to be constant over the whole resonance zone. The specific intensity I is then the sum of these two contributions

$$\begin{aligned}I(r,\mu,\nu_{\rm CMF}) &= \theta(\mu-\mu_c)\cdot I_c\cdot e^{-\widetilde{\tau}_+} + \int_0^{\widetilde{\tau}_+}S_L\cdot e^{-\tau}\mathrm{d}\tau \\ &\approx \theta(\mu-\mu_c)\cdot I_c\cdot e^{-\widetilde{\tau}_+} + S_L\left[1-e^{-\widetilde{\tau}_+}\right]\end{aligned} \tag{31}$$

where θ is the step function. Integration of $I(r,\mu,\nu_{\rm CMF})\cdot\varphi(\nu_{\rm CMF})$ over CMF frequency $\nu_{\rm CMF}$ and angle cosine μ yields the mean line intensity defined in Eq. (1)

$$\widetilde{J}_{\rm SOB} = \widetilde{\beta}_c I_c + (1-\widetilde{\beta}_+ - \widetilde{\beta}_-)S^L. \qquad (32)$$

with the "2nd order escape probabilities" [5]

$$\widetilde{\beta}_+(r) := \frac{1}{2}\int_0^1\int_0^\infty \varphi(\nu_{\rm CMF})\cdot e^{-\widetilde{\tau}_+(r,\mu,\nu_{\rm CMF})}{\rm d}\nu_{\rm CMF}\,{\rm d}\mu\,. \qquad (33)$$

$\widetilde{\beta}_-$ and $\widetilde{\beta}_c$ are defined analogously but as μ integral over $[-1,0]$ and $[\mu_c,1]$, respectively. For $\mu<0$ the optical depth $\widetilde{\tau}_+$ in Eq. (33) has to be replaced by $\widetilde{\tau}_-$ which was defined in analogy to Eq. (29).

A 2nd order Sobolev Approximation *with continuum* can be developed in the same way. This yields a transport equation in analogy to Eq. (11) but with the escape probabilities exchanged by second order quantities. In the following we will compare our numerically derived second order result $\widetilde{J}_{\rm SAC}$ with the first order $\overline{J}_{\rm SAC}$ and the exact solution $\overline{J}_{\rm CMF}$ since all three quantities are corrected for the interaction with the continuum. (Note that the interaction term $\overline{U}$ is only expanded to the first order which, however, has only a small inpact on the result since the terms containing $\overline{U}$ are two decades smaller than the other contributions in Eq. (11)). For simplicity, we will use Eq. (32) to discuss the difference between first and second order approximation.

The strongest influence of the curvature term is found at the thermal point (Fig. 23) where $\widetilde{J}_{\rm SAC}$ shows a well developed local minimum which is not present for the first order result $\overline{J}_{\rm SAC}$. The local minimum of the exact solution $\overline{J}_{\rm CMF}$ is at the same location but less pronounced. The reason for this local minimum of $\widetilde{J}_{\rm SAC}$ at the thermal point is the large positive curvature of the velocity field, i.e. ${\rm d}^2v/{\rm d}r^2>0$, which causes $\widetilde{\tau}_+(\nu_0)\gg\widetilde{\tau}_-(\nu_0)$ (compare Fig. 11). This situation is sketched in Fig. 22b. In addition to the positive curvature of $v(r)$, the inner part of the resonance zone reaches the hydrostatic limit with $v\lesssim v_{\rm therm}$ and the "resonance zone" becomes semi-infinite (i.e. $z_{\rm min}$ is no longer defined) for most frequencies. Therefore, the photons propagating from inside to z_0 are shadowed ($\widetilde{\tau}_+\to\infty$) and the escape probablities $\widetilde{\beta}_c$ and $\widetilde{\beta}_+$ are reduced drastically. On the other hand, the influence of ${\rm d}^2v/{\rm d}r^2$ decreases $\widetilde{\tau}_-$ (compare Fig. 22a and 22b) and hence $\widetilde{\beta}_-$ is increased. In consequence the contribution of the non local radiation, i.e. $\widetilde{\beta}_c I_c$ in Eq. (32), is blocked, while roughly half of the local photons corresponding to the $\widetilde{\beta}_- S_L$ term can still escape if the line is not too strong. This reduces $\widetilde{J}_{\rm SAC}$ at the thermal point compared to *both* its value deep in the photosphere where $\widetilde{J}_{\rm SAC}\approx S_L$ *and* its value just above the thermal point where $\widetilde{J}_{\rm SAC}\approx\widetilde{\beta}_c I_c$ for weak and intermediate lines.

[5] The expression "2nd order escape probability" was introduced by Hummer & Rybicky (1982) who expanded the *source function* to develop an approximate radiative transfer for planar and static atmospheres. In contrast we use the expression "2nd order" with respect to the velocity curvature only.

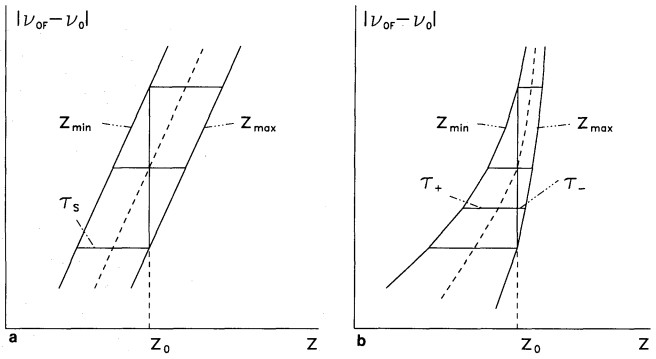

Fig. 22. a and b. Inner (outer) boundary $z_{\rm min}$ ($z$max) of the interaction zone for positive (negative) μ as function of $|\nu_{\rm OF}-\nu_0|$. **a** Case of constant ${\rm d}v/{\rm d}r$ (common assumption in the Sobolev Theory). Note: $\widetilde{\tau}_+ + \widetilde{\tau}_- = \tau_S$. **b** Case of curved velocity field. Note the asymmetry caused by curvature effects

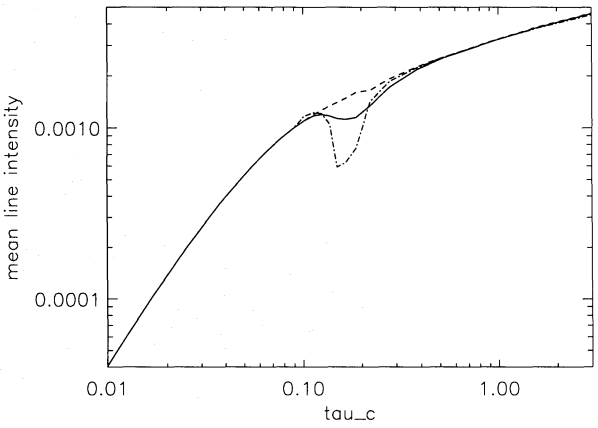

Fig. 23. Mean line intensity $\overline{J}$ in cgs vs. continuum optical depth τ_c for a weak line (He I 4471): first order SAC (dashed), second order SAC concerning the velocity curvature (dashed dotted) and the exact solution in the CMF (solid). The radiation transfer is based on the same occupation numbers for all three cases

This local minimum is not present in the first order mean line intensity $\overline{J}_{\rm SAC}$ because the asymmetric character of the line absorption process at the thermal point is not considered ($\beta_+\equiv\beta_-\equiv\beta/2$). Finally, the exact solution $\overline{J}_{\rm CMF}$ shows a less pronounced minimum than $\widetilde{J}_{\rm SAC}$ since the gradients of χ_L and S_L have not been accounted for.

The inclusion of ${\rm d}\chi_L/{\rm d}r$ by expanding the line opacity in Eq. (29) is straight forward, however the effect on $\overline{J}$ is marginal, independent of whether the velocity curvature is considered or not.

More effort is necessary to investigate the influence of the ${\rm d}S_L/{\rm d}r$ term since then the integral $\int S_L\cdot e^{-\tau}{\rm d}\tau$ cannot be solved using the common analytical method (see Eq. 31). Gradients in the source function were extensively discussed by Castor (1974) in the context of the *line force*, i.e. with respect to the *first moment* of the radiation field. In the present context, however, we are concerned with the *zeroth moment* of the radiation field $\overline{J}$ where the influence of a gradient in S_L cancels

out if a *symmetric* resonance zone is assumed (Fig. 22, case a) because of the funtional dependence $\mathrm{d}S_L/\mathrm{d}z = \mu \cdot \mathrm{d}S_L/\mathrm{d}r$. Including the velocity curvature, however, the situation becomes asymmetric and the gradient of S_L can have a major impact on $\overline{J}$. This is especially the case at the thermal point where the resonance zone is semi-infinite and therefore the increase of S_L towards the inner photosphere fills up the local minimum in $\widetilde{J}_{\mathrm{SAC}}$ to some amout (Fig. 23: compare $\widetilde{J}_{\mathrm{SAC}}$ (dashed dotted) with the exact result $\widetilde{J}_{\mathrm{CMF}}$ (solid)).

Finally, as the run of S_L is non monotonic (see Fig. 13, solid curve), also the inclusion of higher orders would be necessary, so that in consequence a numerical solution is impractical.

Hence, we give the following conclusions for the situation at the thermal point: As it is important to consider the variation of all the quantities $\mathrm{d}v/\mathrm{d}r$, S_L and χ^L, the only correct (and practical) line transfer is the solution in the *comoving frame*. The most important effect on the radiation field is caused by the curvature of the velocity field and the semi-infinite character of the resonance zone for $\mu > 0$ leading to a local minimum in $\overline{J}$.

References

Auer, L.H.: 1991, in *Stellar Atmospheres: Beyond Classical Models*, ed. by L. Crivellari, I. Hubeny and D.G. Hummer, Dordrecht, NATO ASI Series C, vol. 341, p. 9

Bohannan, B., Abbott, D.C., Voels, S.A., Hummer, D.G.: 1986, ApJ 308, 728

Bohannan, B, Voels, S.A., Hummer, D.G.,., Abbott, D.C.: 1990, ApJ 365, 729

Cannon, C.J.: 1973, ApJ 185, 621

Castor, J.I.: 1974, MNRAS 169, 279

Gabler,R., Gabler, A., Kudritzki, R.P., Puls, J., Pauldrach, A.: 1989, A&A 226, 162 (paper I)

Gabler, A., Gabler, R., Pauldrach, A., Puls, J., Kudritzki, R.P.: 1990, in *Properties of Hot Luminous Stars*, ed. by C.D. Garmany, Astronomical Society of the Pacific Conference Series, vol. 7, p. 64

Gabler, R., Kudritzki, R.P., Mendez, R.H.: 1991, A&A 245, 587 (paper II)

Gabler, R., Gabler, A., Kudritzki, R.P., Mendez, R.H.: 1992, A&A in press (paper III)

Hamann, W.-R., Gruschinske, J., Kudritzki., R.P., Simon, K.P.: 1981, A&A 104, 249

Hamann, W.-R.: 1985, A&A 148, 364

Hamann, W.-R., Koesterke, L., Wessolowski, U.: 1991, in *Stellar Atmospheres: Beyond Classical Models*, ed. by L. Crivellari, I. Hubeny and D.G. Hummer, Dordrecht, NATO ASI Series C, vol. 341, p. 191

Heap, S.R., Altner B., Ebbets, D., Hubeny, L., Hutchings, J.B., Kudritzki, R.P., Voels, S.A., Haser, S., Pauldrach A., Puls, J., Butler, K.: 1991, ApJ 377, L29

Hummer, D.G., Rybicki, G.B.: 1982, ApJ 263, 925

Hummer, D.G., Rybicki, G.B.: 1985, ApJ 293, 258

Klein, R.I., Castor, J.I.: 1978, ApJ 220, 902

Kudritzki, R.P., Simon, K.P., Hamann, W.-R.: 1983, A&A 118, 245

Kudritzki, R.P., Hummer, D.G.: 1990, ARA&A 28, 303

Kudritzki, R.P., Hummer, D.G., Pauldrach, W.A., Puls, J., Najarro, F., Imhoff, J.: 1992, A&A 257, 655

Mihalas, D., Kunasz, P., Hummer, D.G.: 1975, ApJ 207, 465

Mihalas, D.: "Stellar Atmospheres", W.H. Freeman and Company, San Francisco, 1978, 2nd edition

Olson, G.L., Auer, L.M., Buchler, J.R.: 1986, *J. Quant. Spectr. Rad. Transfer*, 35, 431

Owocki, S.P.: 1991, in *Stellar Atmospheres: Beyond Classical Models*, L. Crivellari, I. Hubeny and D.G. Hummer, eds., (Kluwer, Dordrecht), 235

Owocki, S.P., Zank, G.P.: 1991, ApJ 368, 491

Pauldrach, A.: 1987, A&A 183, 295

Pauldrach, A., Herrero, A.: 1988, A&A 199, 262

Puls, J., Hummer, D.G.: 1987, A&A 191, 87

Puls, J., Herrero, A.: 1988, A&A 204, 219

Puls, J.: 1991, A&A 248, 581

Rybicki, G.: 1971, *J. Quant. Spect. Rad. Transfer*, 11, 589

Rybicki, G.B., Hummer, D.G.: 1978, ApJ 219, 654

Rybicki, G.B., Hummer, D.G.: 1991, A&A 245, 171

Sobolev,V.V.: 1957, *Soviet Astron. Astrophys. J.*, 1, 678

Voels, S.A., Bohannan, B., Abbott, D.C., Hummer, D.G.: 1989, ApJ 340, 1073

Werner, K., Husfeld, D.: 1985, A&A 148, 417

This article was processed by the author using Springer-Verlag LaTeX A&A style file version 3.